# Enhanced von Weizsäcker Wang-Govind-Carter kinetic energy density functional for semiconductors

Cite as: J. Chem. Phys. **140**, 18A531 (2014); https://doi.org/10.1063/1.4869867
Submitted: 28 December 2013 . Accepted: 18 March 2014 . Published Online: 16 April 2014

Ilgyou Shin, and Emily A. Carter

# Enhanced von Weizsäcker Wang-Govind-Carter kinetic energy density functional for semiconductors

Ilgyou Shin[1] and Emily A. Carter[2,a)]
[1]*Department of Chemistry, Princeton University, Princeton, New Jersey 08544-1009, USA*
[2]*Department of Mechanical and Aerospace Engineering, Program in Applied and Computational Mathematics, and Andlinger Center for Energy and the Environment, Princeton University, Princeton, New Jersey 08544-5263, USA*

(Received 28 December 2013; accepted 18 March 2014; published online 16 April 2014)

We propose a new form of orbital-free (OF) kinetic energy density functional (KEDF) for semiconductors that is based on the Wang-Govind-Carter (WGC99) nonlocal KEDF. We enhance within the latter the semi-local von Weizsäcker KEDF term, which is exact for a single orbital. The enhancement factor we introduce is related to the extent to which the electron density is localized. The accuracy of the new KEDF is benchmarked against Kohn-Sham density functional theory (KSDFT) by comparing predicted energy differences between phases, equilibrium volumes, and bulk moduli for various semiconductors, along with metal-insulator phase transition pressures. We also compare point defect and (100) surface energies in silicon for a broad test of its applicability. This new KEDF accurately reproduces the exact non-interacting kinetic energy of KSDFT with only one additional adjustable parameter beyond the three parameters in the WGC99 KEDF; it exhibits good transferability between semiconducting to metallic silicon phases and between various III-V semiconductors without parameter adjustment. Overall, this KEDF is more accurate than previously proposed OF KEDFs (e.g., the Huang-Carter (HC) KEDF) for semiconductors, while the computational efficiency remains at the level of the WGC99 KEDF (several hundred times faster than the HC KEDF). This accurate, fast, and transferable new KEDF holds considerable promise for large-scale OFDFT simulations of metallic through semiconducting materials. © *2014 AIP Publishing LLC*. [http://dx.doi.org/10.1063/1.4869867]

## I. INTRODUCTION

Computer simulations have steadily evolved over the last few decades as an essential tool in modern materials science.[1] The sustained increase in computational power and efficient algorithm development has enabled the widespread use of first-principles quantum mechanical (QM) methods for materials research. Among various QM methods, Kohn-Sham density functional theory (KSDFT)[2,3] attains a reasonable balance between accuracy and efficiency and is therefore often relied upon for first-principles predictions. Nevertheless, even with its moderate cubic scaling with respect to system size, extensive simulations of thousands of atoms are computationally too demanding. Note that while KSDFT can be made to scale linearly for non-metals,[4] a significant prefactor due to $k$-point sampling makes large scale calculations prohibitively expensive (without using extraordinary computing resources.[5,6])

Orbital-free density functional theory (OFDFT)[7] offers one alternative to KSDFT for large-scale QM simulations. While KSDFT uses single-electron orbitals to evaluate the non-interacting electron kinetic energy, OFDFT uses the electron density as the sole variable in the spirit of the first Hohenberg-Kohn theorem[2] that proves the electron density uniquely determines the ground state properties of a many-electron system. Consequently, the degrees of freedom in OFDFT computations are reduced from $3N$ (due to $N$ KS orbitals for $N$ electrons) to merely 3 spatial coordinates, thereby significantly lowering the overall computational cost. All terms in OFDFT can be made to scale fully quasilinearly $O(N \ln N)$ with system size.[8] Furthermore, the absence of single-electron orbitals eliminates the overhead of $k$-point sampling of the Brillouin zone, which significantly increases the computational cost of KSDFT (especially for metallic systems). Hence, OFDFT can explicitly treat thousands to millions of atoms with first-principles QM accuracy. For example, using parallelization via domain decomposition, a benchmark OFDFT calculation involving more than 1 million Al atoms was demonstrated using a modest number of processors.[8] A number of mesoscale materials properties have been successfully studied with OFDFT: liquid metals,[9–11] vacancy aggregation,[12] nanowire deformation,[13,14] crack tip propagation,[15] and dislocation structure and mobility.[16–18]

Successful OFDFT applications to date have been restricted to nearly-free-electron-like main group metals. This is mainly due to limitations in the kinetic energy density functionals (KEDFs) used in evaluating the electron kinetic energy in OFDFT. Most state-of-the-art OFDFT simulations employ nonlocal KEDFs derived from linear response theory for the perturbed uniform electron gas, namely considering the Lindhard response function,[19] since its exact form is known in

a)Author to whom correspondence should be addressed. Electronic mail: eac@princeton.edu

 

momentum space. These KEDFs include the Chacón-Alvarellos-Tarazona (CAT) KEDF,[20–22] the Wang-Teter (WT) KEDF[23] (and its relatives[24–31] with density-independent kernels), and the Wang-Govind-Carter (WGC99) KEDF[32] with a density-dependent kernel. KEDFs based on higher-order response theories are also available.[23,29,30] Since the Lindhard response function can at best be expected to accurately describe systems with nearly uniform electron densities, these Lindhard-based KEDFs cannot guarantee accuracy for systems with localized electrons.[33] As a result, up to 2005 only very limited progress was made in treating semiconductors or transition metals within OFDFT.[33,34]

Recently, Huang and Carter proposed a new nonlocal KEDF[35] for semiconductors based on the expected asymptotic behavior of a semiconductor's response function. The Huang-Carter (HC) KEDF introduces the reduced density gradient term into the KEDF's kernel as well as two adjustable parameters, one of which is related to the dielectric constant. The HC KEDF accurately reproduces the exact non-interacting kinetic energy of KSDFT for bulk Si and III-V semiconductors[35] and covalently bonded molecules.[36] Although promising, the HC KEDF still has room for improvement for several reasons: (1) it underestimates the electron density in the bonding regions of Si and III-V semiconductors compared to KSDFT predictions; (2) it is less accurate for metallic phases than the WGC99 KEDF, so its transferability from semiconducting to metallic phases is questionable; (3) it incorrectly finds the self-interstitial formation energy for Si to be negative; (4) despite the quasilinear scaling ($O[mNln(N)]$) of the formalism with system size ($N$), a large prefactor ($m = \sim 100$ for bulk Si[35] and much larger for unit cells containing vacuum) prevents its application to larger systems that could be routinely treated by other KEDFs, e.g., the WT and WGC99 KEDFs.

Here we present an improved KEDF for semiconductors. Our objectives were to develop a KEDF that is (1) equally or more accurate than the HC KEDF for various bulk properties and electron densities of Si and III-V semiconductors, (2) as computationally efficient as the WGC99 KEDF (quasilinear scaling with a small prefactor), and (3) transferable between semiconducting and metallic Si phases and for various III-V semiconductors, all with minimal additional parameters. We deemed the WGC99 KEDF a good starting point because it predicts Si's ground state electron density more accurately than the HC KEDF. Furthermore, the WGC99 KEDF is several hundred times faster than the HC KEDF. Although the WGC99 KEDF does not properly describe localized electrons in semiconductors, one ingredient of this KEDF—the von Weizsäcker (vW) KEDF—might do so because it is exact for a single orbital. As chemical bonds typically can be described by a single molecular orbital, local treatment of covalent bonds with the vW KEDF may be the key to improving the accuracy of the WGC99 KEDF when applied to semiconductors. Thus, we propose a new nonlocal KEDF form that enhances the vW KEDF contribution in the WGC99 KEDF. Contemporaneous with the present work, a density decomposition scheme was proposed recently with a similar goal to improve the WGC99 KEDF for covalent materials.[37] The density-decomposed WGC99 (WGCD) KEDF separates the density into localized and delocalized components to which respectively semilocal and the nonlocal WGC99 KEDFs are applied. Here we test the accuracy and efficiency of our new KEDF via extensive benchmarking comparisons against the HC KEDF, the WGCD KEDF, and KSDFT calculations.

To benchmark this new KEDF, we investigated bulk properties of various Si bulk phases, i.e., cubic diamond (CD), hexagonal diamond (HD), complex body-centered-cubic (cBCC), $\beta$-tin, body-centered-tetragonal 5 (BCT5), simple cubic (SC), hexagonal-close-packed (HCP), body-centered-cubic (BCC), and face-centered-cubic (FCC) crystals. We also studied bulk properties of the cubic zincblende (ZB) and hexagonal wurtzite (WZ) structures of the III-V semiconductors AlP, AlAs, AlSb, GaP, GaAs, GaSb, InP, InAs, and InSb. We then calculated vacancy and self-interstitial formation energies of CD Si as well as unreconstructed and reconstructed Si (100) surface energies. Based on these benchmarks, the quality of our new KEDF will be assessed in terms of accuracy, efficiency, and transferability. In what follows, we introduce the theory behind our KEDF in Sec. II, numerical details in Sec. III, results and discussion in Sec. IV, and conclusions are offered in Sec. V.

## II. KINETIC ENERGY DENSITY FUNCTIONAL FORM

According to the first Hohenberg-Kohn theorem,[2] the total electronic energy can be written solely as a functional of the electron density $\rho(\vec{r})$ as

$$E[\rho] = T_S[\rho] + E_{Hart}[\rho] + E_{XC}[\rho] + \int V_{Ext}(\vec{r})\,\rho(\vec{r})\,d\vec{r}, \tag{1}$$

where $T_S[\rho]$ is the kinetic energy of the non-interacting electrons (given as a KEDF in the orbital-free scheme), $E_{Hart}[\rho]$ is the classical Hartree electron-electron repulsion energy, $E_{XC}[\rho]$ is the electron exchange-correlation energy (which also corrects for the kinetic energy of the interacting electrons), and $V_{Ext}(\vec{r})$ is the external potential (typically the ion-electron interaction potential, usually given as a local pseudopotential in an orbital-free scheme). The electron density $\rho(\vec{r})$ is properly normalized to the number of electrons in the system, and it is non-negative in all regions of space. We now describe how $T_s[\rho]$ is evaluated; previous papers present the other terms in detail.[8,16,38]

Although an exact orbital-free KEDF exists in theory, its form is not known except for certain limits. For example, the Thomas-Fermi (TF) KEDF is exact in the limit of a uniform electron gas.[39–41] It has the local functional form

$$T_{TF}[\rho] = C_{TF}\int_{\Omega}\rho(\vec{r})^{5/3}d\vec{r}, \tag{2}$$

where $C_{TF} = \frac{3}{10}(3\pi^2)^{2/3}$ and $\Omega$ is the volume of the unit cell. Likewise, the von Weizsäcker (vW) KEDF is exact for a single orbital system, e.g., for a bosonic ground state or a one-electron or two-electron closed-shell singlet ground state.[42] The vW KEDF has the semi-local functional form

$$T_{vW}[\rho] = \int_{\Omega}\sqrt{\rho(\vec{r})}\left(-\frac{1}{2}\nabla^2\right)\sqrt{\rho(\vec{r})}d\vec{r}. \tag{3}$$

Neither the TF nor the vW KEDF, nor even their linear combinations are sufficiently accurate for real materials.[43] Specifically, such (semi)local KEDFs typically do not reproduce the correct linear response behavior of a uniform electron gas, the so-called Lindhard linear response,[19] which is related to the KEDF at the uniform gas limit by[7]

$$\hat{F}\left(\left.\frac{\delta^2 T_S[\rho]}{\delta\rho(\vec{r})\,\delta\rho(\vec{r}')}\right|_{\rho_0}\right) = -\frac{1}{\chi_{Lind}}. \quad (4)$$

Here $\rho_0$ is the uniform electron gas density and $\hat{F}$ () denotes the Fourier transform. $\chi_{Lind}$ is the Lindhard susceptibility function in reciprocal space, given by

$$X_{Lind} = -\frac{k_F}{\pi^2}\left(\frac{1}{2} + \frac{1-|\vec{\eta}|^2}{4|\vec{\eta}|^2} ln\left|\frac{1+|\vec{\eta}|}{1-|\vec{\eta}|}\right|\right), \quad (5)$$

where $k_F = (3\pi^2\rho_0)^{1/3}$ is the Fermi wavevector of the uniform electron gas and $\vec{\eta} = \vec{q}/2k_F$ is a dimensionless momentum. Wang and Teter (WT)[23] introduced a nonlocal term ($T_{nl}[\rho]$) in the KEDF that explicitly enforces the correct linear response behavior of Eq. (4). The resulting KEDF is

$$T_S[\rho] = T_{TF}[\rho] + T_{vW}[\rho] + T_{nl}[\rho], \quad (6)$$

where $T_{nl}[\rho]$ in the WT KEDF is given as

$$T_{nl}^{WT}[\rho] = C_{TF}\iint \rho^{\alpha}(\vec{r}) w_{\alpha,\beta}(\vec{r}-\vec{r}')\rho^{\beta}(\vec{r}')dr^3dr'^3. \quad (7)$$

Wang, Govind, and Carter (WGC99) improved $T_{nl}[\rho]$ by replacing the density-independent kernel in the $T_{nl}^{WT}[\rho]$ by a density-dependent kernel[32]

$$T_{nl}^{WGC99}[\rho] = C_{TF}\iint \rho^{\alpha}(\vec{r}) w_{\alpha,\beta}(\xi_\gamma(\vec{r},\vec{r}')|\vec{r}-\vec{r}'|)\rho^{\beta}(\vec{r}')dr^3dr'^3, \quad (8)$$

where $\xi_\gamma(\vec{r},\vec{r}') = (\frac{k_F^\gamma(\vec{r})+k_F^\gamma(\vec{r}')}{2})^{1/\gamma}$ and $k_F(\vec{r}) = [3\pi^2\rho(\vec{r})]^{1/3}$ are the nonlocal two-body and local one-body Fermi wavevectors, respectively. $\xi_\gamma(\vec{r},\vec{r}')$ brings a density dependence into the kernel.

These linear-response-based KEDFs are nearly as accurate as the electron kinetic energy in KSDFT for nearly-free-electron-like main group metals, but they are much less accurate for semiconductors. For example, these KEDFs incorrectly predict energy vs. volume relations for semiconducting materials such as CD Si; the WT KEDF does not predict even the presence of stable (covalent) bonding in CD Si (see Figure 1). For localized electrons, such as those in the covalent bonding regions in CD Si, the $T_{vW}[\rho]$ should be able to play a key role in improving the KEDF's accuracy. In this context, we propose a new KEDF form where the $T_{vW}[\rho]$ term is enhanced as

$$T_S[\rho] = (1+A)T_{vW}[\rho] + \left(1-\frac{A}{2}\right)(T_{TF}[\rho] + T_{nl}^{WGC99}[\rho]), \quad (9)$$

and where small portions ($A/2$) of $T_{TF}[\rho]$ and $T_{nl}^{WGC99}[\rho]$ are each replaced by an equal portion ($A/2$) of $T_{vW}[\rho]$. (Because $T_{nl}^{WGC99}[\rho]$ is more accurate than $T_{nl}^{WT}[\rho]$ for semiconductors, we use $T_{nl}^{WGC99}[\rho]$ for the nonlocal term in Eq. (9).)

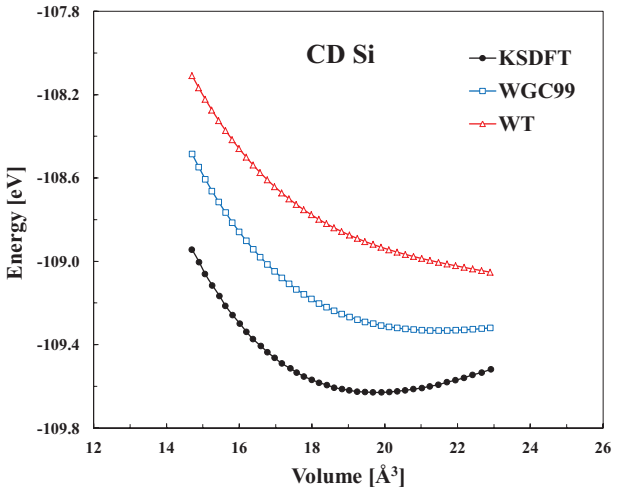


FIG. 1. OFDFT and KSDFT total energy versus volume curves for CD Si. We use the same exponents $\alpha, \beta = \frac{5}{6} \pm \frac{\sqrt{5}}{6}$ for the WT and WGC99 KEDFs. The other parameter $\gamma$ for the WGC99 KEDF is set to 4.2.

The partitioning factor $A$ is a small positive number or zero (Table I). If $A = 0$, then the $T_S[\rho]$ in Eq. (9) recovers the WGC99 KEDF (Eq. (6) with $T_{nl}[\rho] = T_{nl}^{WGC99}[\rho]$) for a nearly-free-electron-like metal. It is expected that the factor $A$ will vary depending on the nature of the material and its electron distribution. We therefore propose $A$ to have the form:

$$A = k\left(\frac{\rho_{max}-\rho_0}{\rho_0}\right)^2, \quad (10)$$

where $k$ is the sole adjustable, material-dependent parameter and $(\frac{\rho_{max}-\rho_0}{\rho_0})^2$ is a volume-dependent, dimensionless quantity indicating the extent to which the electron density is localized anywhere in the system under consideration. $\rho_{max}$ and $\rho_0$ are the maximum and average densities of the system, respectively. We introduce the scaling parameter $k$ anticipating that the $(\frac{\rho_{max}-\rho_0}{\rho_0})^2$ term itself may not be flexible enough to describe electron localization in different bonding environments within a variety of materials. When $k = 0$ or the electron density is uniform (where $\rho_{max} = \rho_0$), then the $T_S[\rho]$ recovers the WGC99 KEDF, which is appropriate for nearly-free-electron-like metals. Different optimal $k$ values can be obtained to reproduce the equilibrium KS kinetic energy for each crystal structure. It is evident that the optimal $k$ value depends on the crystal structure because even for the same element, different crystal structures produce significant differences in material properties. For example, CD Si is semiconducting while FCC Si is metallic, meaning their electron distribution in turn differs significantly. Accordingly, their optimal $k$ values should be different. Indeed, the optimal $k$ values for CD and FCC Si are 0.018 and 0, respectively (Table I). A larger $k$ value for a semiconducting structure compared to a metallic structure is intuitive because larger $k$ (leading to a larger $A$ from Eq. (10)) means more electrons are localized so that the $T_{vW}[\rho]$ is enhanced more in our new KEDF—hereafter referred to as the enhanced vW-WGC (EvW-WGC) KEDF—as shown in Eq. (9). The importance of the $T_{vW}[\rho]$ has recently been highlighted in the development of generalized-gradient-type KEDFs in which the KS kinetic energy functional is

TABLE I. Coordination numbers of various Si phases and nonlocal KEDF parameters: $k$ in the enhanced (E)vW-WGC KEDF (this work); $\lambda$, $\beta$ in the HC KEDF; and $a$, $b$, $m$ in the WGCD KEDF. For our KEDF, the resulting $A$ (from $k$ (opt) and $k$ (uni)) and $(\frac{\rho_{max}-\rho_0}{\rho_0})^2$ at each equilibrium structure are also listed. Our KEDF and the WGCD KEDF contain the WGC99 term with default $\alpha$, $\beta = \frac{5}{6} \pm \frac{\sqrt{5}}{6}$. The other WGC99 parameter $\gamma$ used in the two KEDFs is also listed. WGC99 parameters in the two KEDFs do not change in other tables.

| Si structures | | CD | HD | cBCC | $\beta$-tin | BCT5 | SC | HCP | BCC | FCC |
|---|---|---|---|---|---|---|---|---|---|---|
| Coordination number | | 4 | 4 | 4 | 6 | 5 | 6 | 12 | 8 | 12 |
| EvW-WGC (this work) | $k$ (opt) | 0.018 | 0.018 | 0.0185 | 0.0250 | 0.029 | 0.0127 | 0.013 | 0.012 | 0 |
| | $k$ (scf) | 0.025 | ...[a] | 0.0227 | 0.0230 | 0.032 | 0.0290 | 0.015 | 0.014 | 0 |
| | $k$ (uni) | 0.018 | 0.018 | 0.018 | 0.018 | 0.018 | 0.018 | 0.018 | 0.018 | 0.018 |
| | $A$ (opt) | 0.0738 | 0.0766 | 0.0505 | 0.0126 | 0.0306 | 0.0137 | 0.0022 | 0.0026 | 0 |
| | $A$ (uni) | 0.0738 | 0.0766 | 0.0491 | 0.0091 | 0.0190 | 0.0089 | 0.0030 | 0.0040 | 0.0031 |
| | $(\frac{\rho_{max}-\rho_0}{\rho_0})^2$ | 4.10 | 4.26 | 2.73 | 0.50 | 1.06 | 0.51 | 0.17 | 0.21 | 0.16 |
| | WGC99 $\gamma$ | 4.2 | 4.2 | 4.2 | 4.2 | 4.2 | 4.2 | 4.2 | 4.2 | 4.2 |
| HC[35] | $\lambda$ | 0.01 | 0.01 | 0.01 | 0.0055 | 0.0026 | 0.003 | 0 | 0 | 0 |
| | $\beta$ | 0.65 | 0.65 | 0.65 | 0.65 | 0.65 | 0.65 | 0.65 | 0.65 | 0.65 |
| WGCD[37] | $a$ | 0.864 | 0.864 | 0.864 | 0.864 | 0.864 | 0.864 | 0.864 | 0.864 | 0.864 |
| | $b$ | 0.670 | 0.670 | 0.670 | 0.670 | 0.670 | 0.670 | 0.670 | 0.670 | 0.670 |
| | $m$ | 0.000 | 0.030 | 0.070 | 0.114 | 0.210 | 0.190 | 0.335 | 0.230 | 0.400 |
| | WGC99 $\gamma$ | 3.6 | 3.6 | 3.6 | 3.6 | 3.6 | 3.6 | 3.6 | 3.6 | 3.6 |

[a]Because the second-order WGC99 terms diverge for the HD structure, we cannot obtain an accurate, self-consistent $\rho_{max}$, see text for details.

decomposed into the $T_{vW}[\rho]$ plus a non-negative remainder (the Pauli term).[44] Also, semilocal KEDFs were proposed recently that generalize the $T_{vW}[\rho]$ by introducing a parameter that allows the power of the electron density to vary.[45]

The key element of the EvW-WGC KEDF (the factor $A$) has three variables: $k$, $\rho_0$, and $\rho_{max}$; see Eq. (10). We compare two ways of selecting the parameter $k$: (1) optimal values for each Si phase and III-V ZB semiconductor that reproduce corresponding KS kinetic energies (denoted as "opt" or "scf" in Tables II and III); and (2) a universal value for all Si phases and III-V semiconductors ("uni"), which tests our KEDF's transferability. $\rho_0$ is fixed by the number of electrons and the given volume of the sample, unless the volume changes. For surfaces or molecules, $\rho_0$ is selected as the average density within the sample, excluding vacuum placed in the supercell. Next, we use two methods to evaluate $\rho_{max}$. In

TABLE II. Bulk moduli (B), equilibrium volumes ($V_0$), and equilibrium total energies ($E_0$) per atom for various Si phases calculated within OFDFT by the EvW-WGC KEDF with optimal (opt or scf) or universal (uni) parameters, and by the HC and WGCD KEDFs with their optimal parameters. See text for details about "opt," "scf," and "uni." KSDFT results are given as benchmarks. Energies of all phases other than CD are given relative to the energy of the former. Inaccurate results (errors larger than 15 GPa for B, 1 Å$^3$/atom for $V_0$, 30 meV/atom for $E_0$, or incorrect energy ordering) are emphasized in bold italics for ease of viewing.

| | Method | CD | HD | cBCC | $\beta$-tin | BCT5 | SC | HCP | BCC | FCC |
|---|---|---|---|---|---|---|---|---|---|---|
| B [GPa] | EvW-WGC (opt) | 93 | 107 | 117 | 131 | 92 | 119 | 100 | 112 | 89 |
| | EvW-WGC (scf) | 89 | ... | 117 | 112 | 98 | 119 | 98 | 111 | 95 |
| | EvW-WGC (uni) | 93 | 107 | ***119*** | 134 | 97 | 125 | 96 | 110 | 91 |
| | HC[35] | 97 | 98 | 105 | ***83*** | ***66*** | ***81*** | ***71*** | ***82*** | ***64*** |
| | WGCD[37] | 98 | 102 | 94 | 113 | 92 | 115 | 94 | 102 | 86 |
| | KSDFT[35] | 98 | 99 | 102[a] | 121[a] | 96 | 112 | 91 | 98 | 83 |
| $V_0$ [Å$^3$/atom] | EvW-WGC (opt) | 19.653 | ***18.257*** | 16.597 | 14.341 | 16.600 | 15.563 | 14.034 | 14.425 | 13.936 |
| | EvW-WGC (scf) | 19.812 | ... | 16.698 | 13.935 | 16.632 | 15.813 | 14.148 | 14.496 | 13.936 |
| | EvW-WGC (uni) | 19.653 | ***18.257*** | 16.616 | 14.369 | 16.633 | 15.501 | 14.094 | 14.490 | 14.110 |
| | HC[35] | 19.962 | 19.875 | 18.419 | ***15.662*** | ***19.289*** | 16.082 | 14.445 | 14.565 | 14.412 |
| | WGCD[37] | 19.821 | 19.897 | ***18.574*** | ***15.992*** | ***18.627*** | ***16.908*** | 14.279 | 14.309 | 14.011 |
| | KSDFT[35] | 19.781 | 19.642 | 17.512[a] | 14.655[a] | 16.905 | 15.484 | 14.157 | 14.602 | 14.372 |
| $E_0$ [eV/atom] | EvW-WGC (opt) | − 109.626 | 0.023 | 0.153 | 0.170 | 0.216 | 0.233 | 0.338 | 0.353 | 0.368 |
| | EvW-WGC (scf) | − 109.630 | ... | 0.156 | 0.169 | 0.218 | 0.231 | 0.337 | 0.351 | 0.372 |
| | EvW-WGC (uni) | − 109.626 | 0.023 | 0.164 | ***0.217*** | ***0.321*** | ***0.279*** | 0.326 | 0.335 | ***0.326*** |
| | HC[35] | − 109.624 | 0.007 | 0.141 | 0.170 | ***0.119*** | 0.226 | 0.353 | ***0.334*** | 0.351 |
| | WGCD[37] | − 109.627 | 0.015 | 0.153 | 0.163 | 0.225 | 0.234 | 0.347 | 0.359 | 0.360 |
| | KSDFT[35] | − 109.629 | 0.015 | 0.153[a] | 0.167[a] | 0.215 | 0.229 | 0.340 | 0.351 | 0.381 |

[a]These values are taken from Ref. 37. All other KSDFT values are taken from Ref. 35. The same computational setups were used in Refs. 35 and 37, as verified by test calculations by us.

TABLE III. Adjustable parameters in three nonlocal KEDFs: $k$ in EvW-WGC, $\lambda$, $\beta$ in HC, and $a$, $b$, $m$ in WGCD for ZB III-V semiconductors. The resulting $A$ (from $k$ (opt) and $k$ (uni)) for the EvW-WGC KEDF at each equilibrium structure is also listed.

| ZB III-V semiconductors | | AlP | AlAs | AlSb | GaP | GaAs | GaSb | InP | InAs | InSb |
|---|---|---|---|---|---|---|---|---|---|---|
| EvW-WGC | $k$ (opt) | 0.0322 | 0.0273 | 0.0190 | 0.0303 | 0.0250 | 0.0170 | 0.0343 | 0.0284 | 0.0248 |
| | $A$ (opt) | 0.277 | 0.244 | 0.139 | 0.209 | 0.190 | 0.101 | 0.410 | 0.332 | 0.205 |
| | $k$ (uni) | 0.0180 | 0.0180 | 0.0180 | 0.0180 | 0.0180 | 0.0180 | 0.0180 | 0.0180 | 0.0180 |
| | $A$ (uni) | 0.155 | 0.168 | 0.133 | 0.127 | 0.142 | 0.106 | 0.182 | 0.211 | 0.149 |
| HC[35] | $\lambda$ (opt) | 0.0120 | 0.0125 | 0.0120 | 0.0100 | 0.0130 | 0.0100 | 0.0120 | 0.0142 | 0.0120 |
| | $\beta$ (opt) | 0.845 | 0.825 | 0.750 | 0.791 | 0.783 | 0.720 | 0.885 | 0.875 | 0.810 |
| | $\lambda$ (avg) | 0.01177 | 0.01177 | 0.01177 | 0.01177 | 0.01177 | 0.01177 | 0.01177 | 0.01177 | 0.01177 |
| | $\beta$ (avg) | 0.7143 | 0.7143 | 0.7143 | 0.7143 | 0.7143 | 0.7143 | 0.7143 | 0.7143 | 0.7143 |
| WGCD[37] | $a$ (opt) | 0.822 | 0.840 | 0.840 | 0.847 | 0.823 | 0.865 | 0.810 | 0.813 | 0.830 |
| | $b$ (opt) | 0.699 | 0.656 | 0.677 | 0.655 | 0.732 | 0.629 | 0.700 | 0.703 | 0.668 |
| | $a$ (avg) | 0.835 | 0.835 | 0.835 | 0.835 | 0.835 | 0.835 | 0.835 | 0.835 | 0.835 |
| | $b$ (avg) | 0.679 | 0.679 | 0.679 | 0.679 | 0.679 | 0.679 | 0.679 | 0.679 | 0.679 |

calculations denoted as "opt" and "uni," we evaluate $\rho_{max}$ based on a WGC99 KEDF OFDFT calculation using the same cell. We do not further update $\rho_{max}$ during EvW-WGC OFDFT density optimization so the factor $A$ in Eq. (10) is fixed in each optimization step (see flow chart, Figure 2(A)). If we do not keep $A$ fixed, the line search does not converge properly because the updated $\rho_{max}$ alters $A$ and $T_S[\rho]$ in every step. Alternatively, we can also optimize $\rho_{max}$ self-consistently by optimizing an initial $\rho_{max}$ from the WGC99 KEDF calculation and then updating $\rho_{max}$ after each density optimization loop finishes (see flow chart, Figure 2(B)). We repeat this until both $\rho_{max}$ and the total energy are converged. This evaluation scheme is denoted as "scf." Self-consistently optimizing $\rho_{max}$ requires additional loops so that the overall computation becomes several times slower than the WGC99 KEDF computation. We find that the additional computational cost does not bring much benefit, as the accuracy is about the same regardless of whether self-consistent calculations are used to obtain $\rho_{max}$ (see Table II, *vide infra*). Self-consistent $\rho_{max}$ and WGC99-optimized $\rho_{max}$ values are different, but they end up providing essentially the same $A$ value by using different $k$ values, thus the accuracy of $T_S[\rho]$ remains the same.

It is surely worth attempting to find a single universal parameter $k$ (independent of structure) for each element but formulating this is not easy. Huang and Carter tried to use the same parameters for structures with the same coordination number (CN).[35] For example, CD (CN = 4), HD (CN = 4), and cBCC (CN = 4) Si share the same HC parameters and so do HCP (CN = 12) and FCC (CN = 12) Si. However, some

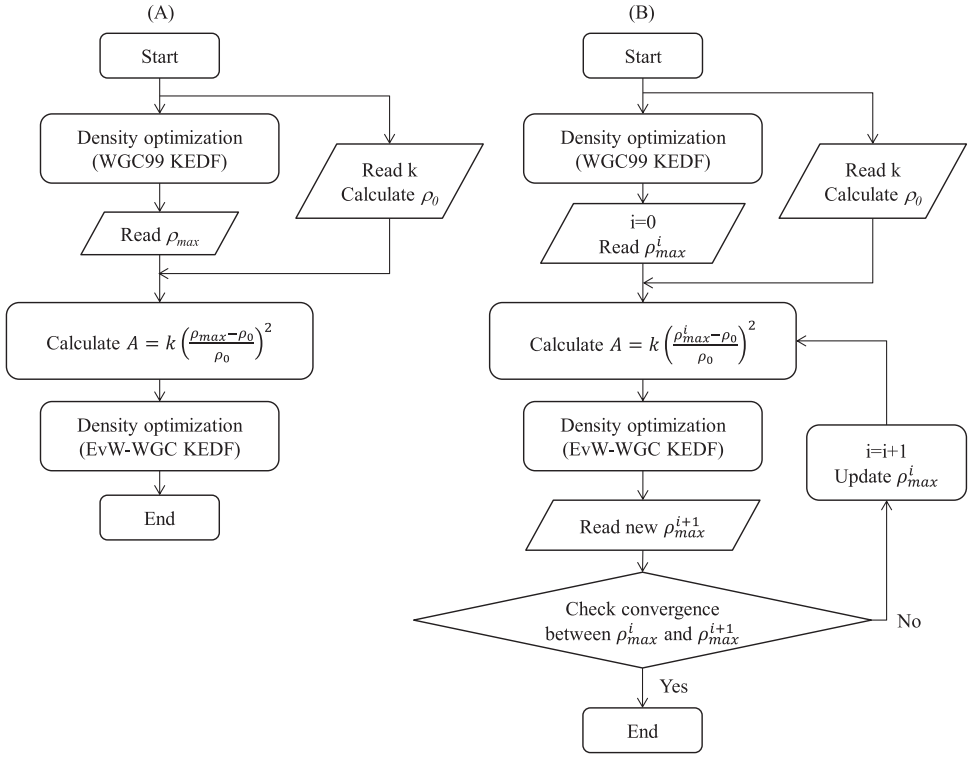


FIG. 2. Flowcharts of two possible procedures for the EvW-WGC KEDF OFDFT calculation.

exceptions were needed, e.g., BCC (CN = 8) Si shared the same parameters as the structures with CN = 12; $\beta$-tin and SC Si have the same CN = 6, but use different parameters; and the parameter for BCT5 (CN = 5) Si was counter-intuitively not in between the values of CN = 4 and CN = 6, etc. One of the optimal WGCD parameters also shows a similar trend:[37] a shift parameter $m$ (*vide infra*) is proportional to CN, except for BCT5. Like the HC parameters, the WGC parameter for BCT5 was not in between the values of CN = 4 and CN = 6.

We therefore tested the EvW-WGC KEDF's transferability with respect to choice of $k$. We set the parameter $k$ to the optimal value of ground state CD Si for all Si structures. The $T_S[\rho]$ using the universal $k$ value cannot be more accurate than using the optimal $k$ value for each structure; however, it is comparably accurate to previous OF KEDFs using their optimal parameters for each structure (Table II, *vide infra*). Reasonably good transferability when using the universal $k$ value implies that the $(\frac{\rho_{max}-\rho_0}{\rho_0})^2$ term can partly handle the structure-dependence of the electron distribution not accounted for by the universal $k$. In principle, we could improve the EvW-WGC KEDF by replacing the $(\frac{\rho_{max}-\rho_0}{\rho_0})^2$ term with a term $F[\rho(\vec{r})]$, which could potentially more accurately characterize the structure- and volume-dependent electron distribution. Unfortunately, an optimal form of the functional $F[\rho(\vec{r})]$ is not known and its density dependence can cause numerical challenges with regard to retaining linear scaling of the nonlocal KEDF term. Finding a better partitioning function $F[\rho(\vec{r})]$ remains an open problem.

## III. NUMERICAL DETAILS

The EvW-WGC KEDF is implemented in PROFESS 2.0 (PRinceton Orbital-Free Electronic Structure Software), a plane-wave-based OFDFT code developed by Carter and coworkers.[8,38,46] OFDFT results in the present work are benchmarked against Huang and Carter's previously reported KS-DFT results[35] and are compared to HC KEDF[35] and WGCD KEDF[37] OFDFT results as well.

We calculate electronic exchange and correlation (XC) using the local density approximation (LDA) derived from the quantum Monte Carlo results of Ceperley and Alder[47] as parameterized by Perdew and Zunger.[48] For the ion-electron interaction, we use bulk-derived local pseudopotentials (BLPSs)[49,50] generated by inverting the KS equations for a target density to obtain the KS effective potential, which is then unscreened with respect to Hartree and XC potentials. We use the densities of various structures as input, obtained from KSDFT with a Troullier-Martins[51] nonlocal pseudopotential. The qualities and construction details of the BLPSs are summarized in previous literature.[35,49,50] Since the main purpose of this paper is to compare our new OF KEDF to KS-DFT kinetic energies, the choice of the LDA XC functional and the BLPS is irrelevant as long as the same ones are used in both the OFDFT and KSDFT calculations.

We use the two universal exponents $\alpha, \beta = \frac{5}{6} \pm \frac{\sqrt{5}}{6}$ for the WGC99 KEDF, determined by asymptotic analysis.[31] The two-body Fermi wave vector mixing parameter $\gamma$ is set to 4.2 for all phases. This value is optimal for ground state CD Si.[38] Since the WGC99 KEDF kernel is density-dependent, computation of the exact convolution scales quadratically. To achieve quasilinear scaling (by using fast Fourier transforms), we perform a Taylor series expansion of the WGC99 KEDF kernel, which factors out the density dependence in the kernel. The Taylor expansion has the form

$$\begin{aligned} & w_{\alpha,\beta}(\xi_\gamma(\vec{r},\vec{r}')|\vec{r}-\vec{r}'|) \\ & = w_{\alpha,\beta}(k_F^*|\vec{r}-\vec{r}'|) \\ & \quad + \left.\frac{\partial w_{\alpha,\beta}(\xi_\gamma(\vec{r},\vec{r}')|\vec{r}-\vec{r}'|)}{\partial\rho(\vec{r})}\right|_{\rho_*} \theta(\vec{r}) \\ & \quad + \left.\frac{\partial w_{\alpha,\beta}(\xi_\gamma(\vec{r},\vec{r}')|\vec{r}-\vec{r}'|)}{\partial\rho(\vec{r}')}\right|_{\rho_*} \theta(\vec{r}') \\ & \quad + \left.\frac{\partial^2 w_{\alpha,\beta}(\xi_\gamma(\vec{r},\vec{r}')|\vec{r}-\vec{r}'|)}{\partial\rho^2(\vec{r})}\right|_{\rho_*} \frac{\theta^2(\vec{r})}{2} \\ & \quad + \left.\frac{\partial^2 w_{\alpha,\beta}(\xi_\gamma(\vec{r},\vec{r}')|\vec{r}-\vec{r}'|)}{\partial^2\rho(\vec{r}')}\right|_{\rho_*} \frac{\theta^2(\vec{r}')}{2} \\ & \quad + \left.\frac{\partial^2 w_{\alpha,\beta}(\xi_\gamma(\vec{r},\vec{r}')|\vec{r}-\vec{r}'|)}{\partial\rho(\vec{r})\partial\rho(\vec{r}')}\right|_{\rho_*} \theta(\vec{r})\theta(\vec{r}') + \cdots, \end{aligned} \tag{11}$$

where $(\vec{r}) = \rho(\vec{r}) - \rho_*$, $k_F^* = (3\pi^2\rho_*)^{1/3}$, and $\rho_*$ is a reference density, generally chosen to be the average electron density of the system. The Taylor expansion can only be evaluated up to second order since the third derivative of the kernel involves the first derivative of the Lindhard function, which has a logarithmic discontinuity at $|\vec{\eta}| = 1$ (see Eqs. (4) and (5)).

The second-order terms in the Taylor expansion of the WGC99 KEDF exhibit numerical instabilities while optimizing densities for hexagonal (HD or WZ) structure semiconductors, ZB InSb, and the Si (100) surface. The EvW-WGC KEDF employing the WGC99 term also has the same numerical instabilities for these semiconductors. Therefore, to estimate the factor $A$ in the EvW-WGC KEDF for hexagonal systems (HD or WZ), we use the WGC99 kernel expanded only through first order, since the first-order terms never diverge. We assume that a good estimate of $\rho_{max}$ can be obtained from

$$\rho_{max}^{(2,Hex)} = \frac{\rho_{max}^{(2,Cub)}}{\rho_{max}^{(1,Cub)}} \times \rho_{max}^{(1,Hex)}, \tag{12}$$

where $\rho_{max}^{(i,Hex)}$ and $\rho_{max}^{(i,Cub)}$mean $\rho_{max}$ of hexagonal (HD or WZ) and cubic (CD or ZB) structures, respectively, optimized by the $i$th order-Taylor-expanded WGC99 KEDF. The ratio of $\rho_{max}$ optimized by the first- and second-order WGC99 KEDF is assumed to be the same for both structures because of the similarity of the two structures (both four-coordinate, covalently bonded). This assumption was verified for HCP and FCC Si, where both first- and second-order kernels are well behaved and so the second-order WGC99 KEDF $\rho_{max}$ can be directly computed for HCP Si and compared to the outcome of Eq. (12): the error is less than 0.05%. $k$ and $\rho_0$ in Eq. (10) are unrelated to the optimization problem, so together with the estimates of Eq. (12), the values of $A$ for hexagonal structures can be determined. This approximation could be

used to perform the second-order WGC99 calculation for any case in which the second-order WGC99 term exhibits numerical instabilities in optimization.

Given the values of $A$, calculations using the new EvW-WGC KEDF can proceed using the full second-order Taylor expansion of the WGC99 KEDF kernel, because the EvW-WGC KEDF resolves the numerical instability problem for WZ AlP, AlAs, GaP, GaAs, InP, and InAs. However, to successfully carry out the second-order Taylor expansion for the other unstable cases (HD Si, WZ AlSb, WZ GaSb, WZ and ZB InSb, and Si(100)), we scale the second-order terms of the Taylor expansion of Eq. (11) by a factor $C$. For systems where the full second-order Taylor expansion diverges, we can converge the electron density by using a $C$ somewhat smaller than 1. Based on data points calculated using several $C$s (e.g., $C = 0.0, 0.2, 0.4, 0.6, 0.8$), we extrapolate to the full second-order Taylor-expanded values (where $C = 1$; Eq. (11)). As a test of this extrapolation procedure, we compared the extrapolated values of the total energy and $\rho_{max}$ to the directly calculated values in CD Si, which has no optimization problem. The error in the extrapolated value is less than 0.01%.

One might ask if this somewhat complex numerical procedure is worth doing, rather than simply using a KEDF that does not require the Taylor expansion. For example, the density optimization problem does not occur in WT-type KEDFs that have a density-independent kernel. However, this family of functionals is much less accurate than the WGC99 KEDF (with its density-dependent kernel) for most properties of semiconductors.[33] Therefore, despite the numerical instability for some systems, we should not to abandon the density dependence in the KEDF kernel.

All OFDFT calculations employ plane wave basis kinetic energy cutoffs of 1600 eV for Si and 2000 eV for III-V semiconductors, which converge the total energies to within 1 meV/cell. (Note that these cutoffs are equivalent to 400 and 500 eV in standard KSDFT codes.) Equilibrium volumes and bulk moduli are calculated by expanding and compressing the optimized lattice parameters by up to about 2.5% to obtain seven energy-volume points. Those are then fit to Murnaghan's equation of state.[52] We also calculate the phase transition pressures based on the common tangent rule,

$$\left.\frac{dE}{dV}\right|_{phase1} = \left.\frac{dE}{dV}\right|_{phase2} = -P_{trans}. \tag{13}$$

Internal atomic coordinates or c/a ratios for hexagonal structures are fixed at the KSDFT-optimized values.[35,36] The first physical flaw of the EvW-WGC KEDF to report is that its use within OFDFT does not yield global minima for the Si HD and BCT5 structures, each of which contain two internal degrees of freedom. We therefore use KSDFT-optimized structures for those phases, as well as for cBCC, $\beta$-tin, and HCP structures for fair comparison.

The vacancy formation energy of CD Si is calculated by removing one corner atom in a $2 \times 2 \times 2$ supercell (eight eight-atom cubic cells). The self-interstitial formation energy of CD Si is calculated by inserting an extra Si atom at a tetrahedral interstitial site in a $2 \times 2 \times 2$ supercell. $\rho_* = \frac{3}{2}\rho_0$ is used for the Taylor expansion of the WGC99 KEDF kernel to more accurately treat the higher electron density around the interstitial atom without encountering numerical instabilities. (The WGC99 kernel showed numerical instabilities with $\rho_* < \frac{3}{2}\rho_0$.) The corresponding energy of the perfect crystal is then calculated with $\rho_* = \frac{3}{2}\rho_0$ for consistency; in each case, $\rho_0$ is defined as the average density of the sample, namely the number of electrons in the cell divided by the cell volume, so $\rho_0$ is higher for the interstitial case than for the perfect crystal, which is turn higher than the vacancy case. The Taylor expansion center $\rho_*$ in the vacancy calculation is just taken as usual to be the average density of the cell appropriate for both cases (with and without the vacancy). The internal coordinates are not relaxed in either the OFDFT or the benchmark KSDFT calculations. The point defect energies are calculated by Gillan's expression,[53]

$$E_{defect} = E\left(N \pm 1, 1, \frac{N \pm 1}{N}\Omega\right) - \frac{N \pm 1}{N} E\left(N, 0, \Omega\right), \tag{14}$$

where $E(N, m, \Omega)$ is the total energy for a cell of volume $\Omega$ with $N$ atoms and $m$ defects. The "+" and "−" sign denotes self-interstitial and vacancy defects, respectively.

Finally, we calculate unreconstructed and reconstructed Si (100) surface energies. The unreconstructed surface structure is modelled by nine unit cell layers with one atom/layer. The surface structure is kept fixed at bulk values using the KSDFT lattice constant. The reconstructed surface structure is fixed at a KSDFT-optimized geometry. The Si(100) surface reconstructs to form Si-Si covalent bonds, which we model using rows of nonalternately buckled dimers, i.e., the $p(2 \times 1)$ surface structure. The periodic slab contains 12 layers and 24 atoms, relaxed with the two middle layers fixed at their equilibrium bulk positions to mimic a semi-infinite crystal field. Both surface structures employed 10 Å of vacuum between periodic slabs. The same surface structure was used to calculate the Si(100) surface energy in Ref. 37. The Taylor expansion center $\rho_*$ and the average density $\rho_0$ were taken to be the same as the $\rho_0$ in bulk CD Si. The surface energy $\sigma$ is calculated from

$$\sigma = \frac{E_{slab} - NE_0}{2A_s}, \tag{15}$$

where $E_{slab}$ is the total energy of the slab, $E_0$ is the energy per atom in equilibrium bulk CD Si, $N$ is the number of atoms in the slab, and $A_s$ is the surface area.

## IV. RESULTS AND DISCUSSION

Our intention for our new KEDF is to preserve or exceed the accuracy of the HC KEDF for various semiconductor properties while retaining the computational efficiency of the WGC99 KEDF (quasilinear scaling without a large prefactor ($O[Nln(N)]$)). We hope the EvW-WGC KEDF proves to be transferable across semiconducting and metallic phases, and offers improved electron density distributions. We benchmark our new KEDF against KSDFT predictions for various properties of Si and III-V semiconductors in what follows. We also compare our KEDF to the HC KEDF and another new WGC99-based KEDF mentioned above, the density-decomposed WGC99 (WGCD) KEDF.[37]

### A. Bulk properties of Si

To investigate the quality of the EvW-WGC KEDF, we first focus on bulk properties (bulk modulus, equilibrium volume, and equilibrium total energy) of various Si phases. Table II compares OFDFT predictions using different KEDFs to illuminate their accuracy relative to KSDFT. OFDFT/HC KEDF and KSDFT data are taken from Ref. 35 while OFDFT/WGCD KEDF results are from Ref. 37. We compare three procedures when using the EvW-WGC KEDF: (1) optimizing the parameter $k$ for each Si structure and using the WGC99-optimized $\rho_{max}$ (opt) for calculating $A$; (2) optimizing $k$ for each Si structure and using the self-consistently optimized $\rho_{max}$ (scf); and (3) using a universal $k$ value (0.018, the optimal value for ground state CD Si) for all Si structures (uni) to test transferability when paired with the WGC99-optimized $\rho_{max}$ for calculating $A$.

The optimal $k$ values for each Si structure are fitted only to the KSDFT equilibrium energies. The bulk modulus and equlibrium volume are not part of the fit and therefore represent a verification test for the KEDF. With optimal parameters (opt and scf), our KEDF agrees very well with KSDFT, except for the equilibrium volume of HD Si (Table II). The two choices for $\rho_{max}$ (opt and scf) yield almost the same accuracy. Although the $(\frac{\rho_{max}-\rho_0}{\rho_0})^2$ terms differ in the two procedures, the resulting $A$ values in Eq. (10) can end up being essentially the same due to the use of different $k$ values. We henceforth use the WGC99-optimized $\rho_{max}$ for further calculations, which is much faster without the additional loops for obtaining a self-consistent $\rho_{max}$. Transferability tests using a universal parameter (uni) will be discussed at the end of this section.

The HC KEDF has two tunable parameters: λ (the coefficient of the density gradient term in the KEDF kernel) and $\beta$ ($\beta$ and 8/3-$\beta$ are the two density exponents in the nonlocal term), and both were fitted to the KSDFT equilibrium energy and volume for CD Si. For other Si structures, only λ was tuned to match the KSDFT equilibrium energies, with $\beta$ fixed at optimal value for CD Si. Unlike EvW-WGC (opt), the HC KEDF does not predict the correct phase ordering for BCT5 and BCC structures. Equilibrium volumes for $\beta$-tin and BCT5 structures are less accurate (significant error for BCT5) and the bulk moduli for $\beta$-tin, BCT5, SC, HCP, BCC, and FCC structures are less accurate than the predictions of our new KEDF.

The WGCD KEDF has three tunable parameters: $a$ and $b$ (the $aT_{TF}[\rho] + bT_{vW}[\rho]$ KEDF is used for interaction and localized density kinetic energy terms) and $m$ (a shift parameter in a numerically constructed scale function used to identify the localized and delocalized densities). $a$ and $b$ were fitted to the KSDFT equilibrium energy and volume for CD Si. For other Si structures, only $m$ was tuned to match the KSDFT equilibrium energies. The WGCD KEDF performs very well overall, except for less accurately predicted equilibrium volumes of cBCC, $\beta$-tin, BCT5, and SC structures.

Enhancement of the $T_{vW}[\rho]$ term significantly improves the quality of the WGC99 KEDF for Si. Optimal $A$ values for the EvW-WGC KEDF are larger for semiconducting structures where electrons are more localized (Table I). For such localized electrons, a larger $A$ value increases the enhancement of the $T_{vW}[\rho]$ term, which is more physically appropriate than the $T_{TF}[\rho]$and $T_{nl}[\rho]$ terms for localized electrons, rendering our new KEDF accurate for semiconductors. By contrast, the optimal $k$ value for FCC Si is zero, which implies that the WGC99 KEDF is already accurate for metallic Si (recall when $k = 0$, the EvW-WGC KEDF reverts to the WGC99 KEDF). This observation suggests that the WGC99 KEDF might reliably treat metallic phases of other non-metals such as metallic carbon nanotubes, though the combination of $\sigma$ and $\pi$-electrons might pose special challenges. Because the EvW-WGC KEDF reverts to the WGC99 KEDF in the metallic limit while being much more accurate than the WGC99 KEDF in the semiconducting limit, we expect the EvW-WGC KEDF might also be able to simulate metal-insulator transitions in materials. An example of its promise for such phenomena is given below, when we examine its ability to describe Si's CD to $\beta$-tin phase transition.

Insight can be gained by comparing $(\frac{\rho_{max}-\rho_0}{\rho_0})^2$ values optimized using the WGC99 KEDF, for each equlibrium structure. This term is clearly structure-dependent, as we anticipated in Sec. II (Table I). It is inversely proportional to the CN, i.e., the number of bonds per atom (Figure 3). In general, the higher the CN, the more the electrons will be delocalized. Therefore $(\frac{\rho_{max}-\rho_0}{\rho_0})^2$ decreases with increasing CN. This term is nearly identical for CD and HD structures, both of which have the same CN (4). Another tetrahedrally coordinated structure, cBCC, has a noticeably smaller value than those of CD and HD. This comparison implies that the electron density is more delocalized in the cBCC structure, consistent with the fact that cBCC Si is metallic, unlike CD and HD Si. This term for BCT5 (CN = 5) is smaller than those for CD, HD, and cBCC (CN = 4) structures, consistent with the expected trend. $\beta$-tin and SC structures (CN = 6) yield nearly the same value, smaller than that of BCT5 (CN = 5), again following the pattern. BCC (CN = 8) then follows $\beta$-tin and SC structures. The smallest value is obtained for HCP and FCC (CN = 12). This consistent trend means the $(\frac{\rho_{max}-\rho_0}{\rho_0})^2$ term captures some aspects of the

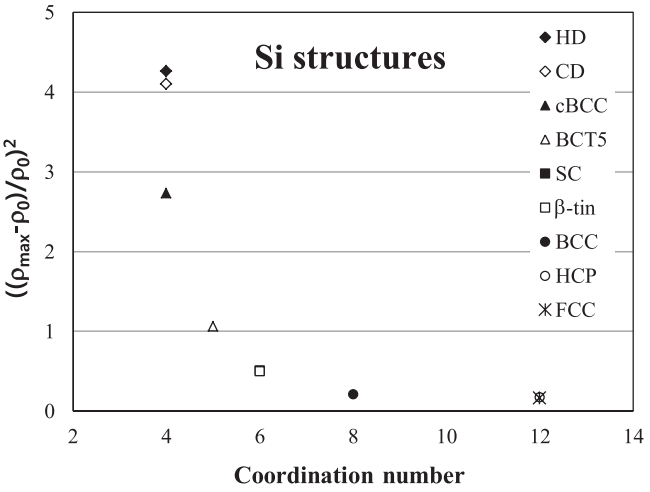


FIG. 3. Coordination number versus $(\frac{\rho_{max}-\rho_0}{\rho_0})^2$ values optimized using the WGC99 KEDF for various Si structures. (■ SC and □ $\beta$-tin are superposed.)

structural dependence; however, the variability in the optimal $k$ value for each structure suggests the $(\frac{\rho_{max}-\rho_0}{\rho_0})^2$ term is not sufficient by itself.

After considering $(\frac{\rho_{max}-\rho_0}{\rho_0})^2$ and optimal $k$ values for different Si structures, an immediate question arises: how accurately can $(\frac{\rho_{max}-\rho_0}{\rho_0})^2$ solely describe the structural dependence of electron densities within the same material? If this single term suffices, we can reduce the number of parameters. In order to test this idea, we benchmark the EvW-WGC KEDF using a universal $k$ value (uni)—the one optimized for ground state CD Si—against KSDFT predictions for Si bulk properties (Table II). Surprisingly, even without parameter fitting, our KEDF is in quite good agreement with KSDFT, except for a few cases. The equilibrium energies of $\beta$-tin, BCT5, and SC are slightly too high, while that of FCC is slightly too low, so that the phase orderings between BCT5 vs. SC and BCC vs. FCC are flipped (however, note the small energy differences); also the equilibrium volume of HD Si and the bulk modulus of cBCC are not accurate. However, for equilibrium volumes, our new KEDF using the universal parameter is more accurate than the HC and WGCD KEDFs that use optimal parameters for each structure. For bulk moduli, the new KEDF with universal $k$ is more accurate than the HC KEDF with optimal parameters but less accurate than the WGCD KEDF with optimal parameters.

The potential power of this new KEDF to describe pressure-induced phase transitions and metal-insulator transitions is illustrated in Figure 4, where we compare total energy versus isotropic volume curves for CD and $\beta$-tin Si calculated within OFDFT using our new KEDF, the HC and WGCD KEDFs, benchmarked against KSDFT. While all three KEDFs within OFDFT reproduce very well the KSDFT curve for CD Si, only our EvW-WGC KEDF does an adequate job treating $\beta$-tin Si compared to KSDFT. The HC and WGCD KEDFs have offset minima and different curvatures from KSDFT, while the EvW-WGC curves have excellent optimal volumes and moduli. Even when a universal parameter is employed in the EvW-WGC KEDF, its E-V curve is much closer to KSDFT's curve than the HC and WGCD KEDFs, even though the latter used parameters optimal for $\beta$-tin rather than universal ones. A stringent test of KEDF transferability is starkly demonstrated by the calculated transition pressures for Si transforming from the CD to the $\beta$-tin structure. If one were to simulate this semiconductor to metal transition in, e.g., a molecular dynamics (MD) simulation, one would have to use the same Hamiltonian to describe their coexistence. In our context, this means we must compare results using the same—universal—set of parameters in the KEDF, unlike what is shown for most of the curves in Figure 4, which employed the optimal KEDF parameters for each phase. Using the same $k$ parameter in the EvW-WGC KEDF (thus all KEDF parameters used are the same) for both phases (the "uni" curve in Figure 4), the transition pressure is predicted to be 6.3 GPa, in good agreement with the KSDFT prediction of 5.4 GPa. In stark contrast, when the same (optimal for CD) parameters are used within the HC and WGCD KEDFs for both phases, they predict unphysical transition pressures of $-2.3$[35] and $-12.0$ GPa,[37] respectively. In other words, the optimal parameters for CD Si do not predict the CD structure as an equilibrium structure. Only when the optimal parameters for each phase are used does one arrive at physically reasonable values for the transition pressure from the HC (6.4 GPa[35]) and WGCD (6.9 GPa[37]) KEDFs. However, it is clearly desireable to have a universal parameter set so that coexistence between phases can be described within the same simulation, which should now be possible with our new EvW-WGC KEDF.

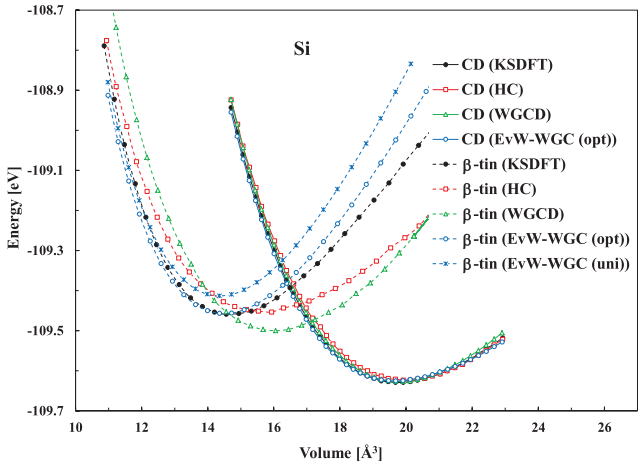


FIG. 4. OFDFT and KSDFT total energy versus volume curves for CD and $\beta$-tin Si. The optimal KEDF parameters for each phase are listed in Table I. Only for the new EvW-WGC KEDF do we show curves with a universal $k$ parameter used for both phases, denoted as EvW-WGC (uni), so that all KEDF parameters are completely the same for both phases.

### B. Bulk properties of III-V semiconductors

As demonstrated above, our new KEDF accurately reproduces KSDFT predictions for bulk properties of various Si phases, from semiconducting to metallic. Next we benchmark our new KEDF for binary III-V semiconductors; see Table III for optimal and universal parameters for the three KEDFs considered. Table IV compares the performance of the EvW-WGC KEDF to the HC and WGCD KEDFs, as well as to KSDFT benchmarks for bulk properties of ZB III-V semiconductors. We fit the parameter $k$ in the EvW-WGC KEDF to the KSDFT equilibrium energies (opt) of the ZB structures. The resulting $A$ values are closely correlated with the KSDFT band gap of each semiconductor (Figure 5). This correlation is intuitive because larger band gaps mean electrons are more localized so that the factor $A$ should become larger. We also find the correlation (quantified by the slopes in Figure 5) between the band gap and the factor $A$ is strongly dependent on which group V atom is under consideration. The slope and the $A$ value are largest for P-based III-V semiconductors and smallest for Sb-based ones. The more polarizable Sb-containing semiconductors have the smallest band gaps and the most delocalized electron distribution, consistent with its smaller values and range of $A$. By contrast, the more localized electron distributions in P- and As- containing semiconductors produce larger band gaps with larger values and range of $A$. In the HC and WGCD KEDF calculations, two parameters ($\lambda$ and $\beta$ in the former; $a$ and $b$ in the latter) were fitted to the KSDFT equilibrium energies and volumes

TABLE IV. Bulk moduli (B), equilibrium volumes ($V_0$), and equilibrium total energies ($E_0$) per cell for various ZB III-V semiconductors calculated within OFDFT by the EvW-WGC KEDF with optimal (opt) or universal (uni) parameters, and by the HC and WGCD KEDFs with optimal (opt) or average (avg) parameters. "avg" is the average value of optimal parameters for CD Si and ZB III-V semiconductors. See text for details about "opt," "uni," and "avg." KSDFT results are listed as benchmarks. Inaccurate results (errors larger than 15 GPa for B, 2 Å$^3$/two-atom cell for $V_0$, 60 meV/two-atom cell for $E_0$ or incorrect energy ordering) are called out in bold italics.

| | Method | AlP | AlAs | AlSb | GaP | GaAs | GaSb | InP | InAs | InSb |
|---|---|---|---|---|---|---|---|---|---|---|
| B [GPa] | EvW-WGC (opt) | 105 | 80 | 59 | 89 | 71 | 61 | 85 | 71 | 42 |
| | EvW-WGC (uni) | 93 | 90 | 54 | 89 | 73 | 57 | 72 | 77 | 48 |
| | HC (opt)[35] | 91 | 76 | 61 | 87 | 81 | 58 | 66 | 63 | 49 |
| | HC (avg)[35] | 89 | 76 | 61 | 94 | 78 | 62 | 68 | 61 | 49 |
| | WGCD (opt)[37] | 94 | 84 | 60 | 80 | 80 | 64 | 70 | 67 | 49 |
| | WGCD (avg)[37] | 95 | 90 | 56 | 90 | 72 | 66 | 69 | 64 | 51 |
| | KSDFT[35] | 90 | 80 | 60 | 80 | 75 | 56 | 73 | 65 | 50 |
| $V_0$ [Å$^3$/cell] | EvW-WGC (opt) | 41.237 | 44.512 | 55.507 | 36.324 | 40.825 | 50.492 | ***48.742*** | 48.579 | ***56.542*** |
| | EvW-WGC (uni) | 41.376 | 44.889 | 55.477 | 37.470 | 42.036 | ***50.399*** | 44.043 | 48.536 | ***58.098*** |
| | HC (opt)[35] | 40.423 | 44.700 | 55.996 | 37.788 | 40.798 | 52.686 | 45.854 | 49.500 | 62.847 |
| | HC (avg)[35] | 40.290 | 44.746 | 55.917 | 36.795 | 41.214 | 51.779 | 45.930 | 50.596 | 62.461 |
| | WGCD (opt)[37] | 40.407 | 45.098 | 55.665 | 37.741 | 40.789 | 52.341 | 46.992 | ***51.259*** | 63.699 |
| | WGCD (avg)[37] | 40.654 | 44.820 | 55.657 | 37.426 | 41.581 | 51.591 | 47.404 | ***51.732*** | 63.520 |
| | KSDFT[35] | 40.637 | 43.616 | 56.607 | 37.646 | 40.634 | 52.488 | 46.040 | 49.123 | 62.908 |
| $E_0$ [eV/cell] | EvW-WGC (opt) | − 240.179 | − 232.904 | − 206.615 | − 243.078 | − 235.798 | − 209.700 | − 235.703 | − 228.527 | − 202.378 |
| | EvW-WGC (uni) | ***−238.603*** | ***−231.948*** | −206.548 | ***−241.952*** | ***−235.174*** | −209.751 | ***−233.509*** | ***−227.127*** | ***−201.900*** |
| | HC (opt)[35] | − 240.199 | − 232.912 | − 206.588 | − 243.057 | − 235.782 | − 209.739 | − 235.696 | − 228.523 | − 202.381 |
| | HC (avg)[35] | ***−238.612*** | ***−231.702*** | ***−206.309*** | ***−242.113*** | ***−235.086*** | −209.686 | ***−233.497*** | ***−226.775*** | ***−201.572*** |
| | WGCD (opt)[37] | − 240.165 | − 232.909 | − 206.607 | − 243.069 | − 235.790 | − 209.705 | − 235.697 | − 228.544 | − 202.382 |
| | WGCD (avg)[37] | ***−239.836*** | ***−232.749*** | ***−206.788*** | ***−243.282*** | ***−236.111*** | ***−210.287*** | ***−234.723*** | ***−227.837*** | ***−202.026*** |
| | KSDFT[35] | − 240.182 | − 232.908 | − 206.606 | − 243.079 | − 235.799 | − 209.697 | − 235.722 | − 228.537 | − 202.387 |

of each semiconductor ground state (opt). We also compare results calculated using the optimal $k$ value for CD Si as a potential universal parameter (uni) for semiconductors. A universal choice of parameters for the other KEDFs was based on average values of the optimal parameters for CD Si and ZB III-V semiconductors (avg).

Comparing our EvW-WGC KEDF (opt) to the HC (opt) and WGCD (opt) KEDFs, the latter two are slightly more accurate for equilibrium volumes, e.g., for GaSb, InP, and InSb, but note the volumes were part of the parameter fit in the HC and WGCD KEDFs. Comparing our KEDF (uni) to the HC (avg) and WGCD (avg) KEDFs, the former tends to be more accurate for total energies and the latter for volumes; however, the overall quality is similar. All three KEDFs reasonably reproduce KSDFT results without parameter adjustment for each III-V semiconductor. Figure 6 further compares the three KEDFs to KSDFT for the total energy versus isotropic volume curves of ZB GaAs. All three of these nonlocal KEDFs reproduce the KSDFT curve remarkably well.

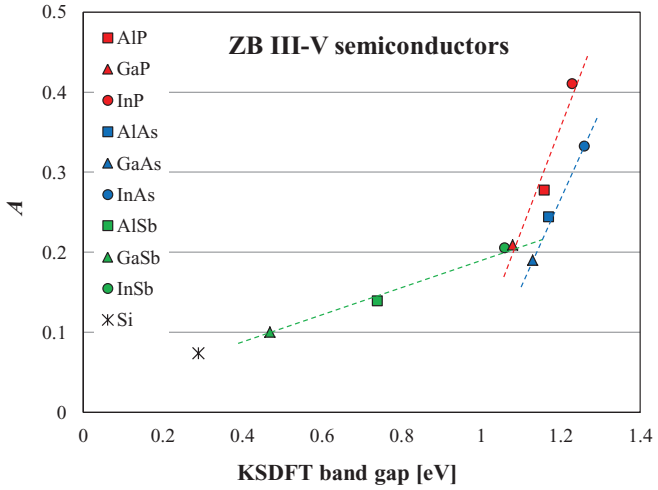


FIG. 5. Correlation between KSDFT band gap[35] and the partitioning factor $A$ ($k(\frac{\rho_{max}-\rho_0}{\rho_0})^2$) for ZB III-V semiconductors.

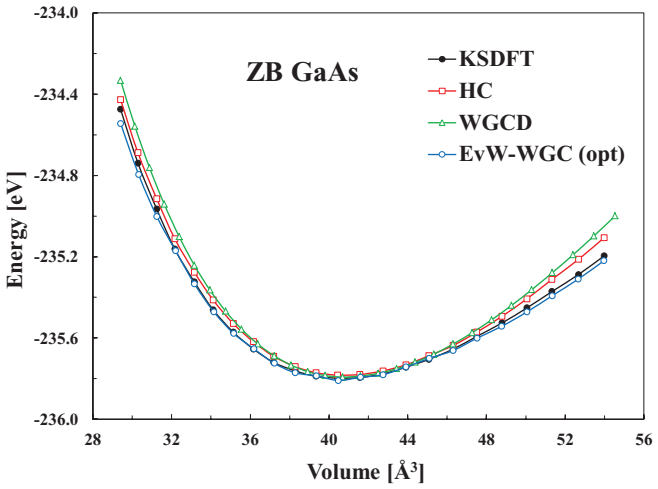


FIG. 6. OFDFT and KSDFT total energy versus volume curves for ZB GaAs. The optimal KEDF parameters used are listed in Table III.

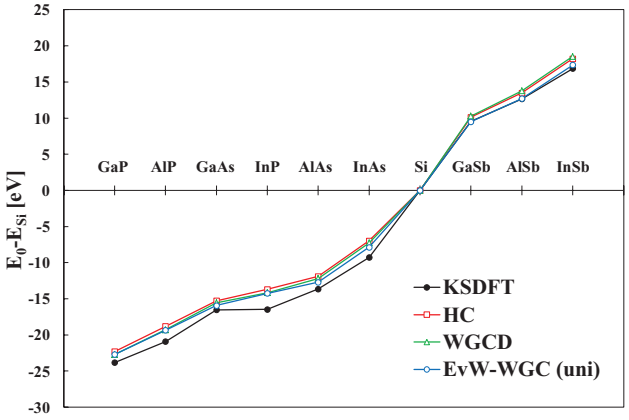


FIG. 7. OFDFT and KSDFT relative energy differences between CD Si and ZB III-V semiconductors. Average or universal KEDF parameters used are listed in Tables I and III.

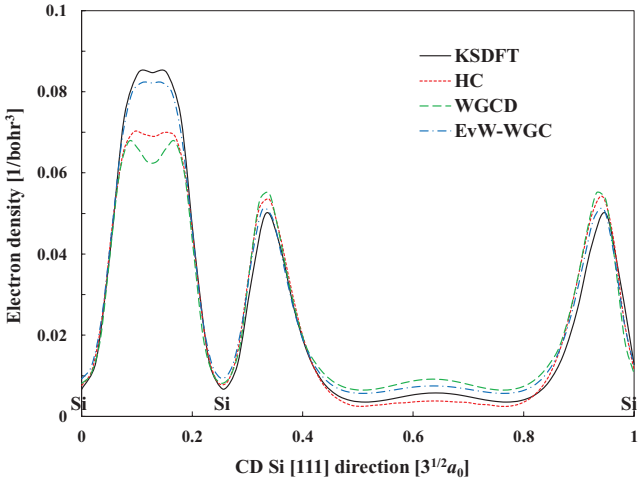


FIG. 8. Electron density of CD Si along the [111] direction. The optimal KEDF parameters used are listed in Table I. The nuclear positions are denoted by element symbols.

To test the transferability of the universal $k$ value, we compare relative energies of ZB III-V semiconductors to the energy of CD Si (Figure 7). The KSDFT energy ordering trends are well reproduced by our KEDF (uni) as well as the HC (avg) and WGCD (avg) KEDFs without parameter adjustment for each semiconductor. Our KEDF is in slightly better agreement with KSDFT than the others.

Finally, we investigate bulk properties of WZ III-V semiconductors (Table V). ZB's optimal parameters for each material are used for all KEDFs. Our KEDF is generally less accurate than the HC and WGCD KEDFs for bulk moduli, equilibrium volumes, and the total energy of InSb. However, the errors are not too large with the EvW-WGC KEDF except for antimony (Sb) compounds, where equilibrium volumes are roughly 10% underestimated. It is not clear at this point what the origin of the problem is with Sb, aside from perhaps some difficult describing the p-electrons of Sb with a KEDF (Sb will s-p hybridize the least of the Group V elements considered).

### C. Electron densities

We further evaluate the quality of our new KEDF by examining the optimized electron density distribution along the [111] direction for CD Si and ZB GaAs. We compare our KEDF results to the HC and WGCD KEDFs and KSDFT benchmarks. Figures 8 and 9 respectively reveal that our KEDF most closely reproduces the electron density of CD Si and ZB GaAs calculated by KSDFT. The predicted electron density of CD Si by our KEDF is significantly more accurate than the HC KEDF in all bonding regions whereas the WGCD KEDF is less accurate than the HC KEDF in all regions. Thus the localized chemical bonds in Si are well reproduced by our new KEDF, while the HC and WGCD KEDFs overdelocalize the density. By contrast, the picture is mixed for ZB GaAs: our new KEDF is more accurate for the first and third highest density regions, the WGCD KEDF is more accurate for the second highest density region, and the HC KEDF is more accurate around the lowest density region.

TABLE V. Bulk moduli (B), equilibrium volumes ($V_0$), and energy differences between the WZ and ZB phases (meV/cell) for various WZ III-V semiconductors. For all OF KEDFs, optimal parameters were used as listed in Table III. (Note that the optimal parameters were fitted based on the total energy of each ZB structure.) KSDFT results are also given. Inaccurate results (errors larger than 15 GPa for B, 2 Å$^3$/two-atom cell for $V_0$, or incorrect energy ordering) are called out in bold italics.

| | Method | AlP | AlAs | AlSb | GaP | GaAs | GaSb | InP | InAs | InSb |
|---|---|---|---|---|---|---|---|---|---|---|
| B [GPa] | EvW-WGC | 84 | 92 | ***81*** | 103 | 89 | 72 | 85 | ***45*** | ***73*** |
| | HC [35] | 92 | 79 | 59 | 76 | 76 | 59 | 73 | 66 | 48 |
| | WGCD[37] | 89 | 82 | 62 | 98 | 77 | 66 | 70 | 63 | 52 |
| | KSDFT[35] | 90 | 80 | 58 | 88 | 76 | 57 | 73 | 65 | 50 |
| $V_0$ [Å$^3$/cell] | EvW-WGC | ***42.679*** | 41.738 | ***51.601*** | 36.038 | 39.747 | ***47.759*** | 47.012 | 50.992 | ***54.504*** |
| | HC[35] | 40.667 | 44.937 | 56.063 | 37.972 | 40.923 | 52.826 | 46.085 | 49.726 | 63.068 |
| | WGCD[37] | 40.956 | 45.148 | 56.159 | 37.803 | 41.956 | 51.996 | 47.578 | ***52.056*** | 63.922 |
| | KSDFT[35] | 40.608 | 43.621 | 56.548 | 37.625 | 40.611 | 52.397 | 46.037 | 49.129 | 62.884 |
| $E_{WZ}$ - $E_{ZB}$ [meV/cell] | EvW-WGC | 12 | 40 | 35 | 37 | 15 | 48 | 13 | 28 | ***−140*** |
| | HC[35] | 22 | 25 | 16 | 26 | 25 | 15 | 19 | 32 | 17 |
| | WGCD[37] | 12 | 55 | 50 | 68 | 61 | 56 | 40 | 39 | 38 |
| | KSDFT[35] | 9 | 11 | 13 | 18 | 19 | 16 | 3 | 7 | 11 |

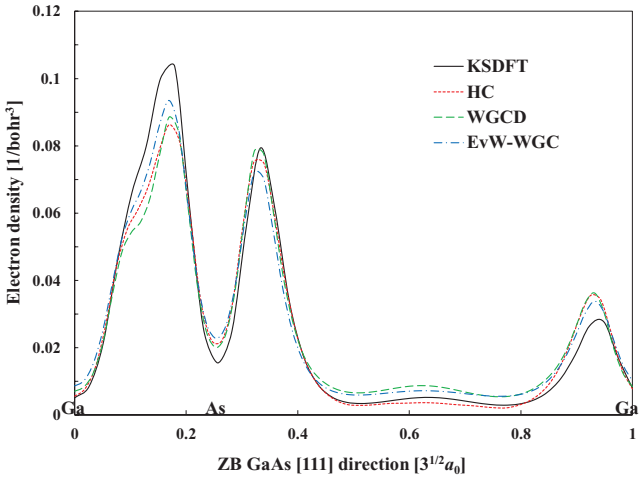


FIG. 9. Electron density of ZB GaAs along the [111] direction. The optimal KEDF parameters used are listed in Table I. The nuclear positions are denoted by element symbols.

It is critical to reproduce accurate electron densities since the OFDFT total electronic energy is expressed completely in terms of the electron density. Electron density in the bonding region is generally the most important because a material's most interesting physical or chemical properties, such as bond formation/breaking or phase transitions, are mainly governed by electrons in the bonding region. The quality of the electron density that the EvW-WGC KEDF produces provides further evidence of the soundness of its underlying physics.

### D. Defect formation energies and Si (100) surface energies

We further test our new KEDF by comparing its CD Si vacancy and self-interstitial formation energy predictions to those of the HC and WGCD KEDFs and KSDFT (Table VI). The HC KEDF predicts a reasonably accurate vacancy formation energy, but it also predicts an unphysical, negative self-interstitial formation energy. The WGCD KEDF significantly underestimates vacancy formation energy and is even worse for the self-interstitial formation energy. Our KEDF predicts the most accurate vacancy formation energy and, more importantly, it predicts a positive self-interstitial formation energy. Although the magnitude is underestimated, our KEDF is the only OF KEDF to date that predicts a physically correct, positive self-interstitial formation energy.

Finally, we calculate the unreconstructed and reconstructed Si(100) surface energies (Table VII). For the former, the surface is frozen in bulk positions. For the latter, we relax the surface within KSDFT and use the KSDFT-relaxed structure within OFDFT calculations for comparison. (The second-order WGC99 term exhibits a numerical instability for optimizing surface structures as mentioned in Sec. III.) Of course, the reconstructed surface energy is lower than its unreconstructed counterpart due to Si-Si bond formation. The former surface energy is predicted to be around half (0.53) the latter surface energy within KSDFT. Our KEDF calculation agrees very well with the KSDFT results for the ratio (0.48) between two surface energies as well as the surface energies themselves. The HC KEDF predicts a reasonably accurate surface energy for the unreconstructed structure (∼8% overestimation); however, the error becomes significantly larger for the reconstructed structure (∼59% overestimation), so that the ratio between two structures is too high (0.78). The WGCD KEDF most accurately predicts both the unreconstructed and reconstructed surface energies, while the ratio between the two surface energies is slightly more underestimated (0.44) than our KEDF.

TABLE VI. CD Si vacancy ($E_{vac}$) and self-interstitial ($E_{si}$) formation energies. The optimal KEDF parameters used are listed in Table I.

| KEDF | $E_{si}$ (eV) | $E_{vac}$ (eV) |
|---|---|---|
| EvW-WGC | 2.85 | 1.17 |
| HC[35] | 2.69 | − 1.91 |
| WGCD[37] | 1.33 | − 6.27 |
| KSDFT[35] | 3.31 | 3.37 |

TABLE VII. Si (100) surface energies ($\sigma_{100}$) for unreconstructed and reconstructed structures. The optimal KEDF parameters used are listed in Table I.

| KEDF | Unreconstructed $\sigma_{100}$ [J/m$^2$] | Reconstructed $\sigma_{100}$ [J/m$^2$] |
|---|---|---|
| EvW-WGC | 2.117 | 1.018 |
| HC[35] | 2.441 | 1.898 |
| WGCD[37] | 2.398 | 1.052 |
| KSDFT[35] | 2.273 | 1.196 |

### E. Computational efficiency

To evaluate computational efficiency of our KEDF, we compare total wall time for optimizing the electron density of CD Si in 1 × 1 × 1 (8 atoms) and 2 × 2 × 2 (64 atoms) cubic supercells, and of FCC Si in a 1 × 1 × 1 (4 atoms) cubic supercell. All calculations are deliberately performed on a single cpu with an unnecessarily large kinetic energy cutoff of 3200 eV, otherwise some calculations finish too quickly. The rest of the computational conditions remain unchanged from those mentioned in Sec. III. Density optimization starts from a uniform density. All KEDFs listed in Table VIII scale quasi-linearly ($O[mNln(N)]$) from the formalism, therefore the difference in efficiency comes from the size of prefactor ($m$) and how many optimization steps are taken. Although the WGC99 KEDF is the most efficient, it is not practically useful because of its low accuracy, as shown in Figure 1. Our EvW-WGC KEDF can be used in two ways, as presented in Figures 2(A) and 2(B). Method (A) needs two density optimization loops, i.e., an initial WGC99 optimization to optimize $\rho_{max}$ followed by a density optimization using the EvW-WGC KEDF. The latter density optimization starts from the optimized density of the former optimization using the WGC99 KEDF, therefore the second optimization needs less optimization steps (generally around half as many as the first optimization that uses the uniform electron density as an initial guess). Since wall time for a single step is almost the same for the WGC99 KEDF and our new KEDF, the total wall time is around 1.5 times

TABLE VIII. Computational wall time, number of truncated Newton (TN) optimization steps, and wall time per step for the WGC99 KEDF, our new EvW-WGC KEDF (with two optimization procedures (A) and (B) in Figure 2), and the HC and WGCD KEDFs.

| | KEDF | CD Si (8 atoms) | CD Si (64 atoms) | FCC Si (4 atoms) |
|---|---|---|---|---|
| Wall time [s] | WGC99 | 20 | 180 | 4 |
| | EvW-WGC (A) | 32 | 288 | 6 |
| | EvW-WGC (B) | 141 | 1416 | 18 |
| | HC | 8664 | 130701 | 178 |
| | WGCD | 38 | 347 | 9 |
| Number of TN optimization steps | WGC99 | 12 | 13 | 8 |
| | EvW-WGC (A) | 19 | 20 | 12 |
| | EvW-WGC (B)[a] | 93 (9) | 102 (9) | 35 (4) |
| | HC | 56 | 206 | 5 |
| | WGCD | 23 | 23 | 14 |
| Wall time for a single TN step [s] | WGC99 | 1.7 | 13.8 | 0.5 |
| | EvW-WGC (A) | 1.7 | 14.0 | 0.5 |
| | EvW-WGC (B) | 1.5 | 13.9 | 0.5 |
| | HC | 154.7 | 634.5 | 35.6 |
| | WGCD | 1.7 | 15.1 | 0.6 |

[a]The number of additional outer loops for self-consistently optimizing $\rho_{max}$ is shown in parentheses; thus the number of TN steps per outer loop is roughly 10.

larger in our KEDF (A) calculation. A KEDF (B) calculation (Figure 2(B)) needs additional SCF loops for optimizing $\rho_{max}$ self-consistently (roughly ∼5 times more density optimization steps are needed for 64 CD Si atoms compared to method (A)), therefore the overall computation is accordingly ∼5 times slower than our KEDF (A) calculation. Comparing our KEDF (A) and the HC KEDF calculations with 64 CD Si atoms, the latter is 454 times slower than the former in terms of the total wall time elapsed. The latter KEDF needs ∼10 times more steps to converge. Even if one improves the optimization algorithm for the HC KEDF calculation so that two KEDFs need the same number of optimization steps, the HC KEDF is still ∼45 times slower than our new KEDF. The HC KEDF has a much larger prefactor for systems with defects or surfaces than bulk CD Si due to the way in which the KE integrals are evaluated, while the efficiency of our KEDF remains unchanged for such systems. Lastly, the WGCD KEDF calculations are about as efficient as our KEDF (A) caluclations, since the most time-consuming nonlocal terms in the two KEDFs are the same.

## V. CONCLUSIONS

Herein we proposed a new OF KEDF for semiconductors. By using a partitioning factor, we enhance the semilocal vW term (exact in the single orbital limit) and suppress the TF term (exact in the uniform electron gas limit) and the nonlocal term (derived from linear response of the perturbed uniform electron gas) in the WGC99 KEDF. This partitioning factor is explicitly related to how markedly the electron density is localized in the system of interest. We also show that this factor is strongly correlated to a material's band gap. By construction the EvW-WGC KEDF seamlessly recovers the uniform gas limit for metallic systems, and benchmarks here have shown that the transition of Si from a semiconducting phase (CD) to a metallic phase ($\beta$-tin) can be accurately described using one universal KEDF. This example could be considered a touchstone to show that metal-insulator transitions can be finally modeled by a universal OF functional.

The accuracy of our EvW-WGC KEDF was benchmarked against KSDFT by comparing predicted energy differences between phases, equilibrium volumes, and bulk moduli for various semiconductors. Our KEDF was frequently more accurate than previously proposed KEDFs for semiconductors, especially for bulk properties of various Si phases. Our new KEDF was also more accurate than the HC and WGCD KEDFs for Si point defect energies, while our new KEDF and the WGCD KEDF were more accurate than the HC KEDF for surface energies. The accuracy of our KEDF for III-V semiconductors was similar to the other KEDFs for ZB structures but less accurate for WZ structures, with Sb being the most difficult element to treat with our KEDF for reasons yet to be revealed. Our KEDF also showed better transferability than the HC and WGCD KEDFs. Our KEDF predicted equilibrium volumes and bulk moduli for various Si phases more accurately than the other KEDFs without any parameter adjustment for each phase, correctly reproducing the phase transition pressure predicted by KSDFT for Si transforming from the semiconducting CD to the metallic $\beta$-tin structure. The Hohenberg-Kohn theorem tells us of the one-to-one correspondence between the ground state density and all physical properties, so simultaneous prediction of accurate physical properties and accurate electron densities must be demonstrated for a well-founded theory. Our KEDF most closely reproduced the electron densities of CD Si and ZB GaAs when compared against KSDFT benchmarks. In addition to accuracy, efficiency of the new KEDF is of course crucial. Our new KEDF is more than two orders of magnitude faster than the HC KEDF, similar to the WGCD KEDF in terms of performance.

Based on these extensive tests, our new EvW-WGC KEDF shows a clear improvement in accuracy, transferability, and efficiency compared to previous OF KEDFs, further advancing the reliability and feasibility of OFDFT to

perform large-scale quantum simulations of semiconductors. However, challenges remain, particularly with some structural optimization cases. The divergence problem encountered in the second-order WGC99 KEDF kernel prevents its use for optimizing hexagonal/wurtzite structures and surface structures as of now. Our next effort will be to resolve this divergence problem so that our new KEDF can be successfully used for optimizing very complex semiconductor structures.

## ACKNOWLEDGMENTS

We are grateful to the Office of Naval Research for funding this work and to Princeton University for supercomputing time. We also thank Junchao Xia and Dr. Youqi Ke for helpful discussions, and Dr. Mohan Chen, Dr. John A. Keith, and Dr. Youqi Ke for critically reading the paper.

[1]E. A. Carter, Science **321**, 800 (2008).
[2]P. Hohenberg and W. Kohn, Phys. Rev. **136**, B864 (1964).
[3]W. Kohn and L. J. Sham, Phys. Rev. **140**, A1133 (1965).
[4]D. R. Bowler, J. L. Fattebert, M. J. Gillan, P. D. Haynes, and C. K. Skylaris, J. Phys.: Condens. Matter **20**, 290301 (2008).
[5]F. Shimojo, R. K. Kalia, A. Nakano, K. Nomfura, and P. Vashishta, J. Phys.: Condens. Matter **20**, 294204 (2008); F. Shimojo, R. K. Kalia, A. Nakano, and P. Vashishta, Phys. Rev. B **77**, 085103 (2008).
[6]A. Nakano, R. K. Kalia, K. Nomura, A. Sharma, P. Vashishta, F. Shimojo, A. C. T. van Duin, W. A. Goddard, R. Biswas, D. Srivastava, and L. H. Yang, Int. J. High Perform. Comput. Appl. **22**, 113 (2008).
[7]Y. A. Wang and E. A. Carter, "Orbital-free kinetic energy density functional theory," in *Theoretical Methods in Condensed Phase Chemistry*, Progress in Theoretical Chemistry and Physics, edited by S. D. Schwartz (Kluwer, Dordrecht, 2000), p. 117–184.
[8]L. Hung and E. A. Carter, Chem. Phys. Lett. **475**, 163 (2009).
[9]B. J. Jesson and P. A. Madden, J. Chem. Phys. **113**, 5924 (2000).
[10]D. J. Gonzalez, L. E. Gonzalez, and M. J. Stott, Phys. Rev. B **74**, 014207 (2006).
[11]M. Chen, L. Hung, C. Huang, J. Xia, and E. A. Carter, Mol. Phys. **111**, 3448 (2013).
[12]G. Ho, M. T. Ong, K. J. Caspersen, and E. A. Carter, Phys. Chem. Chem. Phys. **9**, 4951 (2007).
[13]G. Ho and E. A. Carter, J. Comput. Theor. Nanosci. **6**, 1236 (2009).
[14]L. Hung and E. A. Carter, J. Phys. Chem. C **115**, 6269 (2011).
[15]L. Hung and E. A. Carter, Modell. Simul. Mater. Sci. Eng. **19**, 045002 (2011).
[16]I. Shin, A. Ramasubramaniam, C. Huang, L. Hung, and E. A. Carter, Philos. Mag. **89**, 3195 (2009).
[17]I. Shin and E. A. Carter, Modell. Simul. Mater. Sci. Eng. **20**, 015006 (2012).
[18]I. Shin and E. A. Carter, Phys. Rev. B **88**, 064106 (2013).
[19]J. Lindhard, Kgl. Danske Videnskab. Selskab Mat.-Fys. Medd. **28**, 8 (1954).
[20]E. Chacón, J. E. Alvarellos, and P. Tarazona, Phys. Rev. B **32**, 7868 (1985).
[21]P. García-González, J. E. Alvarellos, and E. Chacón, Phys. Rev. B **53**, 9509 (1996).
[22]P. García-González, J. E. Alvarellos, and E. Chacón, Phys. Rev. B **57**, 4857 (1998).
[23]L.-W. Wang and M. P. Teter, Phys. Rev. B **45**, 13196 (1992).
[24]M. Pearson, E. Smargiassi, and P. A. Madden, J. Phys.: Condens. Matter **5**, 3221 (1993).
[25]F. Perrot, J. Phys.: Condens. Matter **6**, 431 (1994).
[26]E. Smargiassi and P. A. Madden, Phys. Rev. B **49**, 5220 (1994).
[27]M. Foley, E. Smargiassi, and P. A. Madden, J. Phys.: Condens. Matter **6**, 5231 (1994).
[28]E. Smargiassi and P. A. Madden, Phys. Rev. B **51**, 117 (1995).
[29]M. Foley and P. A. Madden, Phys. Rev. B **53**, 10589 (1996).
[30]B. J. Jesson, M. Foley, and P. A. Madden, Phys. Rev. B **55**, 4941 (1997).
[31]Y. A. Wang, N. Govind, and E. A. Carter, Phys. Rev. B **58**, 13465 (1998); **64**, 129901(E) (2001).
[32]Y. A. Wang, N. Govind, and E. A. Carter, Phys. Rev. B **60**, 16350 (1999); **64**, 089903(E) (2001).
[33]B. Zhou, V. L. Ligneres, and E. A. Carter, J. Chem. Phys. **122**, 044103 (2005).
[34]B. Zhou and E. A. Carter, J. Chem. Phys. **122**, 184108 (2005).
[35]C. Huang and E. A. Carter, Phys. Rev. B **81**, 045206 (2010).
[36]J. Xia, C. Huang, I. Shin, and E. A. Carter, J. Chem. Phys. **136**, 084102 (2012).
[37]J. Xia and E. A. Carter, Phys. Rev. B **86**, 235109 (2012).
[38]G. Ho, V. L. Ligneres, and E. A. Carter, Comput. Phys. Commun. **179**, 839 (2008).
[39]L. H. Thomas, Proc. Cambridge Philos. Soc. **23**, 542 (1927).
[40]E. Fermi, Rend. Accad. Naz. Lincei **6**, 602 (1927).
[41]E. Fermi, Z. Phys. **48**, 73 (1928).
[42]C. F. von Weizsäcker, Z. Phys. **96**, 431 (1935).
[43]W. Yang, Phys. Rev. A **34**, 4575 (1986).
[44]V. V. Karasiev, R. S. Jones, S. B. Trickey, and F. E. Harris, "Recent advances in developing orbital-free kinetic energy functionals," *New Developments in Quantum Chemistry*, edited by J. L. Paz and A. J. Hernandez (Transworld Research Network, Kerala, India, 2009).
[45]D. García-Aldea and J. E. Alvarellos, Phys. Chem. Chem. Phys. **14**, 1756 (2012).
[46]L. Hung, C. Huang, I. Shin, G. Ho, V. L. Ligneres, and E. A. Carter, Comput. Phys. Commun. **181**, 2208 (2010).
[47]D. M. Ceperley and B. J. Alder, Phys. Rev. Lett. **45**, 566 (1980).
[48]J. P. Perdew and A. Zunger, Phys. Rev. B **23**, 5048 (1981).
[49]B. Zhou, Y. A. Wang, and E. A. Carter, Phys. Rev. B **69**, 125109 (2004).
[50]C. Huang and E. A. Carter, Phys. Chem. Chem. Phys. **10**, 7109 (2008).
[51]N. Troullier and J. L. Martins, Phys. Rev. B **43**, 1993 (1991).
[52]F. D. Murnaghan, Proc. Natl. Acad. Sci. U.S.A. **30**, 244 (1944).
[53]M. J. Gillan, J. Phys.: Condens. Matter **1**, 689 (1989).